SDSS'Rio 2010 STABILITY AND DUCTILITY OF STEEL STRUCTURES
E. Batista, P. Vellasco, L. de Lima (Eds.)
Rio de Janeiro, Brazil, September 8 - 10, 2010

FE MODELLING OF SLENDER CONCRETE-FILLED STAINLESS STEEL TUBULAR COLUMNS UNDER AXIAL COMPRESSION

Zhong Tao*, Brian Uy and Lin-Hai Han*****

* School of Engineering, University of Western Sydney, Penrith South DC, NSW 1797, Australia
College of Civil Engineering, Fuzhou University, Fujian Province, 350108, P.R. China
e-mail: z.tao@uws.edu.au

** School of Engineering, University of Western Sydney, Penrith South DC, NSW 1797, Australia
e-mail: b.uy@uws.edu.au

*** Department of Civil Engineering, Tsinghua University, Beijing, 100084, P.R. China
e-mail: lhhan@tsinghua.edu.cn

Keywords: Concrete-filled steel tubes (CFST), Stainless steel, Slender columns, Strength, Nonlinear analysis, Initial imperfection.

Abstract. *This paper is concerned with the finite element (FE) modelling of slender concrete-filled stainless steel tubular columns (CFSST) under axial compression. This modelling is performed using ABAQUS, a commercially available FE program. Generally good agreement is achieved between the test and predicted results in terms of load-deformation curves and ultimate strength. This demonstrates that the FE modelling presented in this paper can be used with confidence to carry out extensive parametric studies into the behaviour of slender CFSST columns.*

1 INTRODUCTION

Concrete filled steel tubular (CFST) columns have many design and construction merits, and are gaining popularity in buildings, bridges and other types of structures, especially in Australia, China and Japan [1]. Composite construction ideally combines the advantages of both steel and concrete, namely the speed of construction, high strength, and light weight of steel and the inherent mass, stiffness, damping, and economy of concrete.

In recent times, there is an accelerating interest in the use of stainless steel in construction throughout the world. This is attributed to the fact that stainless steel is extremely durable, corrosion resistant, fire resistant and easily maintainable [2]. Previous major projects to have utilized stainless steel include the 300 m tall St Louis, Missouri, USA (1966), the 81 m tall Parliament House Flag Pole in Canberra, Australia (1988) and the Hearst Tower at 959 Eight Avenue, New York City, USA (2006) [3]. Due to the merits of stainless steel, it is evident that it has a very important role to play in the future design of structures, particularly when architects and structural engineers become more cognisant of the need for life cycle costing.

Previous research achievements on stainless steel have demonstrated that stainless steel exhibits fundamentally different material behaviour from carbon steel, such as non-linear stress-strain characteristics, varying elastic modulus, higher residual stresses and improved thermal properties [4]. Therefore, it is expected that the behaviour of stainless steel CFSTs also differs from that of conventional carbon steel CFST columns. Some recent research [5]-[7] carried out has clearly indicated this.

A literature review showed that no research work conducted on slender CFSST columns has been reported. In practice, columns are usually subjected to the influence of slenderness. In this regard, a research program was carried out recently at the University of Western Sydney to investigate the

behaviour of slender CFSST columns. Test results of 24 composite columns with different tube shapes comprised of stainless steel have been reported elsewhere [8]. Finite element (FE) modelling is carried out in this paper to simulate the slender CFSST columns under axial compression, which may be used to conduct further parametric studies.

2 FINITE ELEMENT MODELLING

2.1 General

FE software ABAQUS [9] was used to investigate the buckling behaviour of slender CFSST columns. Because symmetry was assumed, only half of a column was modelled as shown in Figure 1(a). Four-code doubly curved general-purpose shell elements S4R with three translation and three rotation degrees of freedom at each node were used to model the steel tube, whilst 8-node brick elements (C3D8R) with three translation degrees of freedom at each node were used to model the concrete core.

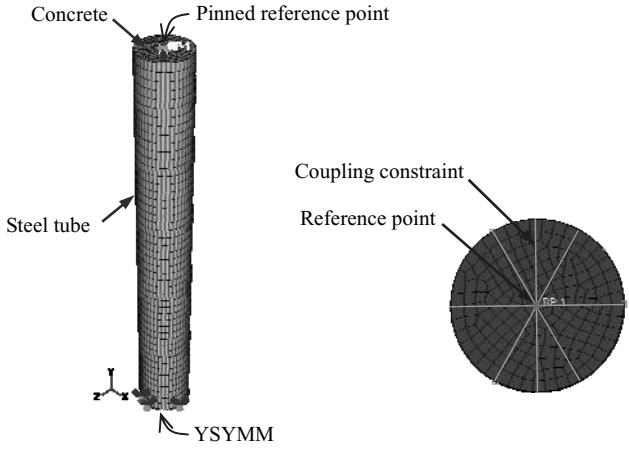

(a) A general view (b) Top surface

Figure 1: Typical finite element model used.

Surface-based contact was used to model the interaction between the stainless steel tube and its core concrete. This model has been used successfully in the past to simulate both CFST columns [10]-[11] and CFSST stub columns [12]-[13]. More details can be found in these references.

As pointed out by Gardner and Nethercot [14], residual stresses cause only a small reduction in initial stiffness but have little influence on the overall load-deformation response for a stainless steel column. Since the influence of residual stresses will be further minimised for a CFST column by concrete filling [11], the residual stresses were not included in the following analysis with an aim to reduce computational time.

2.2 Boundary conditions

To create a pin-ended column model, the cross-section centroid of the top end of the column was defined as a reference point for loading as shown in Figure 1(a). A coupling constraint shown in Figure 1(b) was defined to constrain the motion of the top surface to that of the single reference point, where all three translational degrees of freedom were specified. In this case, all coupling nodes on the top surface follow the rigid body motion of the reference point [9]. All translational degrees of freedom of the reference point, except the vertical displacement, were fixed. Loading was applied in a displacement

control mode at the reference point to simulate the axial loading condition. Symmetry plane at the column mid-height was specified for the FE model (indicated in Figure 1(a) as YSYMM), where the nodes in the symmetry plane were restrained against displacement in the *Y*-direction, as well as the rotational degrees of freedom about the *X* axis and the *Z* axis.

2.3 Material modelling

About the material modelling of stainless steel, a modified Ramberg-Osgood model proposed by Rasmussen [4] is used in this paper. This is based on a model comparison presented by Tao et al. [13]. It was found that the Rasmussen's model can reproduce the actual behaviour of stainless steel even up to relatively high strains of general structural interest. As far as the concrete modelling is concerned, an equivalent stress-strain model proposed by Han et al. [10] has been used, in which the yield strength (f_y) for carbon steel was replaced by the 0.2% proof stress ($\sigma_{0.2}$) for stainless steel.

Since the majority of square and rectangular stainless steel hollow sections are currently formed by cold rolling, the significant strength enhancement at corner regions of cold-formed sections should be considered in FE modelling. Cruise and Gardner's model [15] expressed by Eq. (1) was used to predict the enhanced corner material strength.

$$\sigma_{0.2,c} = \frac{1.673\sigma_{0.2,v}}{(r_i / t)^{0.126}} \tag{1}$$

where $\sigma_{0.2,c}$ and $\sigma_{0.2,v}$ are the 0.2% proof stresses of the corner material and the virgin material, respectively, r_i is the internal corner radius, and t is the thickness of the cross-section. This model has been verified by a large number of published test data [15].

2.4 Initial imperfections

This paper focuses only on CFSST columns with stocky cross-sections, and no local buckling is expected to occur for them before their maximum strengths are attained. In this case, initial local imperfections have only minor influence on the column behaviour. Therefore, the initial local imperfections are not included in the current models to improve computational efficiency.

Global geometric imperfection is essential for a column to be included in its FE model, which is represented by a half-wave sine curve along the column length. Generally, measured out-of-straightness can be used to represent the imperfection amplitude (w_0). According to Young and Ellobody [16] and Ellobody [17], the average measured imperfections of L/1715 and L/5614 are used, respectively, to model slender cold-formed stainless steel unstiffened and stiffened columns, where L is the column length. Based on 12 test results of pin-ended stainless steel column, Gardner and Nethercot [14] conducted a comparative research using three imperfection amplitudes: L/1000, L/2000 and L/5000. An imperfection amplitude w_0 of L/2000 was then recommended by Gardner and Nethercot [14] following parametric studies and comparison with test results. Eight circular and six square cold-formed stainless steel columns were tested by Rasmussen and Hancock [18]. The measured geometric imperfections for the circular columns ranged from L/2000 to L/6667 with an average of L/3496, whilst those for the square columns ranged from L/1429 to L/20000 with an average of L/2233. To predict column curves for stainless steel columns, a global imperfection amplitude of L/1500 was adopted by Rasmussen and Rondal [19], which was based on a mean value of L/1470 for carbon steel columns as suggested by Bjorhovde [20].

From the above review, it is clear that initial global imperfections vary randomly among different supplied tubes. In general, the range of the initial global imperfections is from L/1000 to L/10000. As far as the cold-formed stainless steel tubes presented by Uy et al. [8] are concerned, Measurement was carried out with an aim to obtain geometric imperfections using a stretching metal wire and a Vernier caliper. It appears from the results that these tubes were almost ideally straight, and no visible imperfections could be measured. Therefore, to simulate the CFSST columns presented in [8], w_0 was taken as L/10000 to represent nearly perfect columns [19].

According to the test observations presented by Uy et al. [8], deflection for a rectangular column was mainly observed along the major axis of its cross-section. Therefore, its global imperfection was only applied along the major axis. But the tendency of deflection development was different for a square column since there was no identification of minor or major axis. Without specific indication, global imperfection will only be applied along a principal axis for a square column in the following.

2.5 Mesh convergence studies

Mesh convergence studies were conducted to determine optimal FE mesh that provides relatively accurate solution with low computational time. It was found that the aspect ratio of elements has neglectable influence on the axial load (N) versus lateral mid-height deflection (u_m) curves if this ratio is smaller than 3. Therefore, element size in the axial direction was selected as 2 times that in the lateral direction. An example of convergence study conducted for a square column S1-2a presented by Uy et al. [8] is shown in Figure 2, where the predicted peak strengths based on different refinement meshes are presented. It is clear that finer mesh will give higher strength prediction, but resulting in longer computational time. It seems that the mesh with 5445 elements can give generally good convergence prediction for the specimen S1-2a with acceptable computational time. Based on the mesh convergence studies, element size across the cross-section can be chosen as $D/12$ for a circular column or $B/10$ for a square or rectangular column, where D is the overall diameter of the circular column, and B is the overall width of the square or rectangular column.

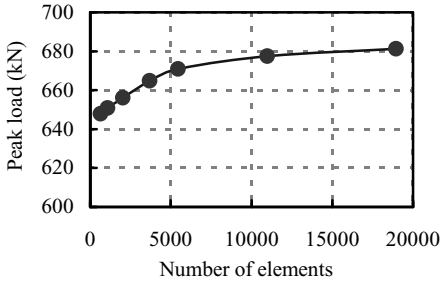

Figure 2: Mesh convergence study for a square specimen S1-2a [8].

3 MODEL VERIFICATION

Twenty four test results of CFSST columns presented by Uy et al. [8], including 12 circular, 6 square and 6 rectangular specimens, respectively, were used to verify the FE models. The specimen details are given in Table 1, where N_{ue} is the measured peak load, L_e is the effective length of a column, f_c' is the cylinder compressive strength of concrete, and H is the overall depth of a rectangular steel tube.

The predicted ultimate loads (N_{uc}) are compared with those obtained from the tests (N_{ue}) in Table 1 and Figure 3, and part test curves are compared with the predicted N-u_m curves in Figure 4. In Figure 3, N_{ue}/N_{uc} is plotted against the slenderness ratio (λ), which is defined as $4L_e/D$ for circular columns, and $2\sqrt{3}L_e/B$ for square or rectangular columns. The mean values of N_{ue}/N_{uc} for the circular, square and rectangular columns are 1.140, 1.053 and 1.086, respectively; whilst the corresponding standard deviations are 0.190, 0.111 and 0.042, respectively.

From the above comparisons, it is clear that the FE predictions are generally conservative compared with the test results, where only three specimens shown in Table 1 have peak loads lower than the predicted results. The largest deviation of the three unconservative predictions is -2.7% for the short circular column C1-1a. It should be noted that very conservative predictions with N_{ue}/N_{uc} larger than 1.25 are achieved for two circular specimens C1-3b and C2-3a, and the square specimen S1-3a. Obviously, these specimens are the slenderest in each section series, but they were tested under nearly perfect axial

compression with much smaller lateral defections developed than expected before their peak loads were reached. Therefore, the second-order effect in these cases is less significant than expected. If ignoring these three specimens, the FE modelling with the values of w_0 taken as L/10000, give reasonable predictions shown in Table 1, where the mean values of N_{ue}/N_{uc} for the circular and square columns are 1.062 and 1.008, respectively.

Table 1: Comparison between FE results and test result.

Section type	No.	Specimen label	$D(B)$ (mm)	H (mm)	t	L_e (mm)	λ	$\sigma_{0.2}$ (MPa)	f_c' (MPa)	N_{ue} (kN)	N_{uc} (kN)	$\frac{N_{ue}}{N_{uc}}$
Circular	1	C1-1a	113.6	–	2.8	485	17.1	288.6	36.3	738.0	758.4	0.973
	2	C1-1b	113.6	–	2.8	485	17.1	288.6	75.4	1137.1	1028.5	1.106
	3	C1-2a	113.6	–	2.8	1540	54.2	288.6	36.3	578.9	555.1	1.043
	4	C1-2b	113.6	–	2.8	1540	54.2	288.6	75.4	851.1	820.9	1.037
	5	C1-3a	113.6	–	2.8	2940	103.5	288.6	36.3	357.6	346.6	1.032
	6	C1-3b	113.6	–	2.8	2940	103.5	288.6	75.4	731.8	498.9	1.467
	7	C2-1a	101	–	1.48	440	17.4	320.6	36.3	501.3	486.3	1.031
	8	C2-1b	101	–	1.48	440	17.4	320.6	75.4	819.0	739.0	1.108
	9	C2-2a	101	–	1.48	1340	53.1	320.6	36.3	446.0	387.8	1.150
	10	C2-2b	101	–	1.48	1340	53.1	320.6	75.4	692.9	616.0	1.125
	11	C2-3a	101	–	1.48	2540	100.6	320.6	36.3	383.0	240.9	1.590
	12	C2-3b	101	–	1.48	2540	100.6	320.6	75.4	389.7	383.2	1.017
Square	13	S1-1a	100.3	–	2.76	440	15.2	390.3	36.3	767.6	761.8	1.008
	14	S1-1b	100.3	–	2.76	440	15.2	390.3	75.4	1090.5	1098.7	0.993
	15	S1-2a	100.3	–	2.76	1340	46.3	390.3	36.3	697.3	708.4	0.984
	16	S1-2b	100.3	–	2.76	1340	46.3	390.3	75.4	1022.9	1011.1	1.012
	17	S1-3a	100.3	–	2.76	2540	87.7	390.3	36.3	622.9	488.7	1.275
	18	S1-3b	100.3	–	2.76	2540	87.7	390.3	75.4	684.2	655.2	1.044
Rectangular	19	R1-1a	49	99.5	1.93	440	31.1	363.3	36.3	385.6	371.3	1.039
	20	R1-1b	49	99.5	1.93	440	31.1	363.3	75.4	558.3	533.0	1.047
	21	R1-2a	49	99.5	1.93	740	52.3	363.3	36.3	361.1	335.2	1.077
	22	R1-2b	49	99.5	1.93	740	52.3	363.3	75.4	517.7	472.1	1.097
	23	R1-3a	49	99.5	1.93	1340	94.7	363.3	36.3	262.8	227.7	1.154
	24	R1-3b	49	99.5	1.93	1340	94.7	363.3	75.4	332.8	301.8	1.103

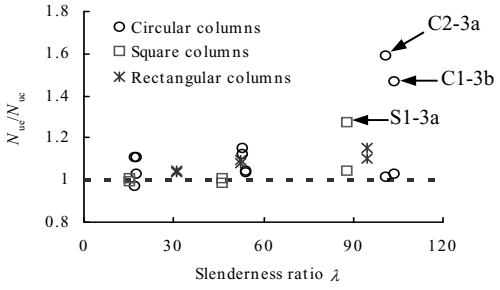

Figure 3: Comparison between predicted and experimental ultimate loads.

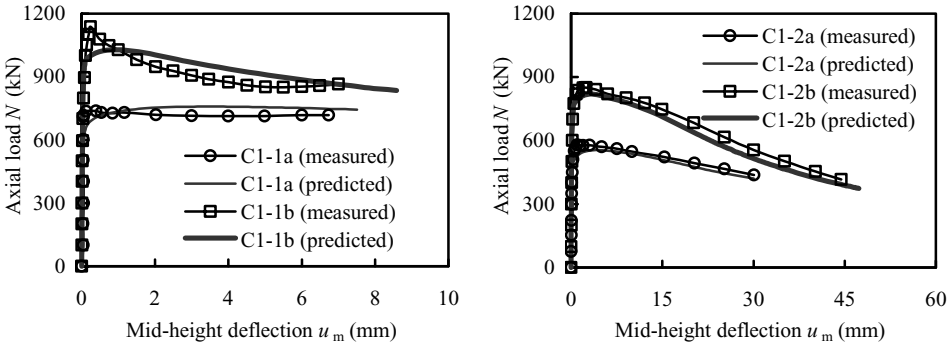

(a) Circular columns (λ=17.1) (b) Circular columns (λ=54.2)

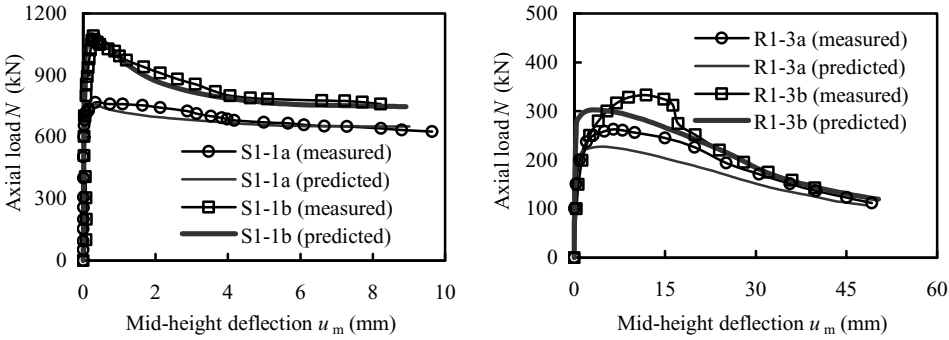

(c) Square columns (λ=15.2) (d) Rectangular columns (λ=94.7)

Figure 4: Comparison between predicted versus experimental N-u_m curves.

The predicted failure modes are also compared with those observed from the tests. Figure 5 shows a comparison between the numerical deformed shapes and the experimental ones presented by Uy et al. [8] for two typical specimens with different cross-sections. To make the comparison more clear, visualisation aid of mirrors provided by ABAQUS was used to produce a desired view of complete models. From the comparison, it can be found that the predicted failure modes also agree well with the tests.

4 CONCLUDING REMARKS

Finite element modelling of slender concrete-filled stainless steel tubular columns under axial compression was performed in this paper, in which nonlinear material behaviour, enhanced strength corner properties of steel, and initial geometric imperfections were all included. Generally good agreement was achieved between the test and FE results in terms of load-deformation response and ultimate strength.

The finite element modeling presented in this paper can be further used to perform a parametric analysis to compare the behaviour of stainless steel CFST columns with that of carbon steel CFST columns. Thus, the behaviour differences between stainless steel and carbon steel CFST columns can be further recognised.

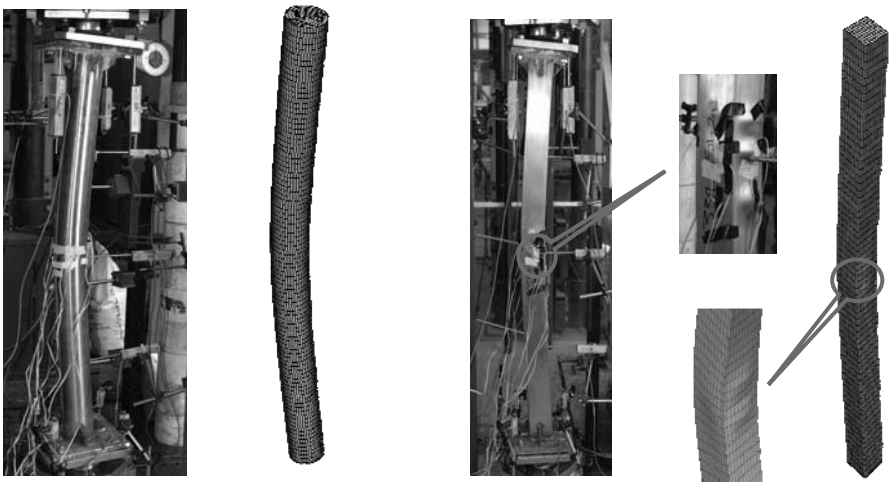

(a) Circular column (C1-2a) (b) Square column (S1-2a)

Figure 5: Comparison between predicted and experimental failure modes.

ACKNOWLEDGEMENTS

This work is part of a project supported by the Australian Research Council (ARC) under its Future Fellowships scheme (Project No: FT0991433). Zhong Tao is the recipient of the Fellowship. This research work has also been partially supported by the Research Grant Scheme and the International Research Initiatives Scheme provided by the University of Western Sydney. This financial support is gratefully acknowledged.

REFERENCES

[1] Tao, Z., Uy, B., Han, L.H. and He, S.H., "Design of concrete-filled steel tubular members according to the Australian Standard AS 5100 model and calibration". *Australian Journal of Structural Engineering*, **8**(3), 197-214, 2008.

[2] Gardner, L., "The use of stainless steel in structures". *Progress in Structural Engineering and Materials*, **7**(2), 45-55, 2005.

[3] Uy, B., "Stability and ductility of high performance steel sections with concrete infill". *Journal of Constructional Steel Research*, **64**(7-8), 748-754, 2008.

[4] Rasmussen, K.J.R., "Full-range stress-strain curves for stainless steel alloys". *Journal of Constructional Steel Research*, **59**(1), 47-61, 2003.

[5] Young, B. and Ellobody, E., "Experimental investigation of concrete-filled cold-formed high strength stainless steel tube columns". *Journal of Constructional Steel Research*, **62**(5), 484-492, 2006.

[6] Lam, D. and Gardner, L., "Structural design of stainless steel concrete filled columns". *Journal of Constructional Steel Research*, **64**(11), 1275-1282, 2008.

[7] Uy, B., Tao, Z. and Han, L.H., "Behaviour of concrete-filled stainless steel tubular columns, Part I-Short columns". *Journal of Constructional Steel Research* (submitted for publication).

[8] Uy, B., Tao, Z. and Han, L.H., "Behaviour of concrete-filled stainless steel tubular columns, Part II-Slender columns". *Journal of Constructional Steel Research* (submitted for publication).

[9] ABAQUS, *ABAQUS Standard User's Manual, Version 6.7.2*, Dassault Systèmes Corp., Providence, RI, USA, 2007.

[10] Han, L.H., Yao, G.H. and Tao, Z., "Performance of concrete-filled thin-walled steel tubes under pure torsion". *Thin-Walled Structures*, **45**(1), 24-36, 2007.

[11] Tao, Z., Uy, B., Han, L.H. and Wang, Z.B., "Analysis and design of concrete-filled stiffened thin-walled steel tubular columns under axial compression". *Thin-Walled Structures*, **47**(12), 1544-1556, 2009.

[12] Ellobody, E. and Young, B. "Design and behaviour of concrete-filled cold-formed stainless steel tube columns". *Engineering Structures*, **28**(5), 716-728, 2006.

[13] Tao, Z., Uy, B., Liao, F.Y. and Han, L.H., "Finite element modelling of concrete-filled square stainless steel tubular stub columns under axial compression", *Proceedings of the 5th International Symposium on Steel Structures*, Seoul, Korea, 87, 2009 (full paper on CD-Rom).

[14] Gardner, L. and Nethercot, D.A., "Numerical modelling of stainless steel structural components—A consistent approach". *Journal of Structural Engineering*, ASCE, **130**(10), 1586-1601, 2004.

[15] Cruise, R.B. and Gardner, L., "Strength enhancements induced during cold forming of stainless steel sections". *Journal of Constructional Steel Research*, **64**(11), 1310-1316, 2008.

[16] Young, B. and Ellobody, E., "Column design of cold-formed stainless steel slender circular hollow sections". *Steel & Composite Structures*, **6**(4), 285-302, 2006.

[17] Ellobody, E., "Buckling analysis of high strength stainless steel stiffened and unstiffened slender hollow section columns". *Journal of Constructional Steel Research*, **63**(2), 145-155, 2007.

[18] Rasmussen, K.J.R. and Hancock, G.J., "Design of cold-formed stainless steel tubular members. I: Columns". *Journal of Structural Engineering*, ASCE, **119**(8), 2349-2366, 1993.

[19] Rasmussen, K.J.R. and Rondal, J., "Column curves for stainless steel alloys", *Journal of Constructional Steel Research*, **54**(1): 89-107, 2000.

[20] Bjorhovde, R., *Deterministic and probabilistic approaches to the strength of steel columns*, PhD dissertation, Lehigh University, PA, 1972.